Journal of Molecular Graphics and Modelling 86 (2019) 256–263

Contents lists available at ScienceDirect

Journal of Molecular Graphics and Modelling

journal homepage: www.elsevier.com/locate/JMGM

A systematic *ab initio* optimization of monohydrates of $HCl \bullet HNO_3 \bullet H_2SO_4$ aggregates

Marian Verdes [1]

Autonomous University of Madrid, Sciences Faculty, Applied Physical Chemistry Department, C-14 Avda. Tomas y Valiente, 7, Cantoblanco, 28049, Madrid, Spain

ARTICLE INFO

Article history:
Received 27 June 2018
Received in revised form
3 October 2018
Accepted 27 October 2018
Available online 31 October 2018

Keywords:
Hydrogen bonds
Electronic structures
Hexagonal shapes
DFT
Aug-cc-pVTZ
B3LYP
Atmospheric aggregates
Nucleation reactions
Aerosols
Astrophysics
Optics
Catalysis
Corrosion of metals and ceramics
Aromatic compounds reactions
Environment pollution
Industrial smog

ABSTRACT

Hydrates of HCl, HNO_3 and H_2SO_4 involved in polar stratospheric clouds capture the attention of researchers due to the mixtures composed with them. The molecular aggregates generated with these strong acids show different behaviors, geometries and nucleation reactions at atmospheric temperatures. Here is presented a systematic *ab initio* optimization study of monohydrates of $HCl \bullet HNO_3 \bullet H_2SO_4$ using the Density Functional Theory, by means of geometry optimizations carried out with B3LYP hybrid method and aug-cc-pVTZ basis set, a high level of theory, within Gaussian 09 program. This systematic optimization procedure consists to situate systematically the H_2O molecule around the cluster in study, on the favorable positions to develop higher quantity of hydrogen bonds as possible, in order to obtain major quantity of different electronic structures of these monohydrates.

Applying this systematic optimization methodology over previously optimized complexes of HCl, HNO_3 and H_2SO_4, the present theoretical approach provides thirty-two different optimized electronic structures of monohydrates that were yielded from seven initial groups of $(HCl \bullet HNO_3 \bullet H_2SO_4)$-complex, placing the H_2O in eight positions around them. Moreover, their Infrared spectra have been predicted for all $(HCl \bullet HNO_3 \bullet H_2SO_4)$-monohydrates achieved. Likewise, It is shown the outcomes of the electronic energies, relative Gibbs free energies, Infrared spectra, the wavenumbers of hydrogen bonds, intermonomeric parameters, electronic structures of $(HCl \bullet HNO_3 \bullet H_2SO_4)$-monohydrates. These monohydrates could be considered precursors of the atmospheric heterogeneous nucleation reactions. These results can be useful to experimentalists of Catalysis, Astrophysics, Corrosion of metals and ceramics, aromatic compounds reactions, even environmental pollution and industrial smog.

1. Introduction

Atmospheric particles formed in Antarctic stratosphere, have been experimentally studied, to explain the formation and composition of polar stratospheric clouds (PSCs). These particles are composed initially by HNO_3 and H_2O with admixture of HCl and H_2SO_4 solutions. Their physical chemistry behavior suggests that the growth of these atmospheric aerosols composed by HNO_3 solutions starts between 200 K and 185 K [1]. On the other hand, H_2SO_4 aqueous solutions was experimentally measured to found their freezing points regarding their concentrations. This research suggested that the formation of ice crystals in cirrus and PSCs are the result of the condensations of H_2O vapor, following of freezing of aerosols with H_2SO_4 [2]. The HNO_3 monohydrate (NAM) was theoretically calculated using *ab initio* quantum chemical methods to found its optimized electronic structure. The NAM remained stable during *ab initio* molecular dynamics developed at 195 K of temperature [3]. The aerosol dynamics of $H_2O–H_2SO_4–HNO_3$ mixtures were formed by homogeneous nucleation, and by absorption, on emitted soot particles by aircrafts. In this research, was investigated the composition and size of the $H_2O–H_2SO_4–HNO_3$ clusters [4].

Moreover, structures as ionic clusters isolated were studied in aqueous HNO_3 and H_2SO_4 solutions by means of electrospray mass spectrometer to assess the conductivity. The protons released from HNO_3 have hopped and delocalized among the water clusters being the cluster structure independent of concentration of the HNO_3. However, the protons of H_2SO_4 not hopping among water clusters

E-mail addresses: marian.verdes@hotmail.com, mariaangeles.verdes@alumni.uam.es.
[1] Tel.: +34 606 411 111, +34 91 497 44 49.

https://doi.org/10.1016/j.jmgm.2018.10.025
1093-3263/

and they would be localized in the self-association clusters of H_2SO_4 under high concentration of H_2SO_4 [5]. A kinetic model for uptake of HNO_3 and HCl on ice is a coated wall flow system tested by simulating experimental results. The analysis has suggested that the ice surface characterized by sites of different binding energy, some weakly bound sites from in which the acid molecules desorbed rapidly, and some strong binding places, which led to irreversible uptake. It is possible that the weakly bound fraction of HNO_3 is interacting with dangling OH bonds. Experiments involving competitive co-adsorption of HNO_3 and HCl conducted at relatively high equilibrium surface coverage well simulated by the model. The presence of strongly bound HNO_3 could modify the reversible adsorption of HCl in contrast to its uptake on fresh ice [6]. On the one hand, the HNO_3/H_2O mixture has been evaluated for its hydrates [mono- (NAM), di- (NAD), tri- (NAT)] in different fields as Infrared spectra (IR), structures, etc. experimental and theoretically [3,7–12]. On the other hand, the H_2SO_4/H_2O systems were analyzed regarding structures, spectra, hydrates, nucleation reactions …, as first step to know the atmospheric behavior [13–20]. Moreover, the ternary mixtures of HCl-HNO_3-H_2O, HNO_3-H_2SO_4-H_2O, HCl-HNO_3-H_2SO_4 and HCl-H_2SO_4-HNO_3 have been investigated —theoretical and experimentally— to looking for the reaction of nucleation: heterogeneous/homogeneous, structures, spectra, vibrational frequencies, hydrogen bonds (HB) [21–36].

Despite of years of research there are questions unanswered regarding atmospheric nucleation processes. For this reason, the aim of this theoretical work is to establish a systematic optimization method to achieve different optimized electronic structures, which will help to experimental researchers to discern which have involved in nucleation reactions in the stratosphere. Besides, this research will be useful to understand the mechanisms exactly of such processes like environmental pollution, catalytic effects, industrial smog, corrosion of metals and ceramics and reactions with organic compounds (aromatic compounds), in the future.

The purpose of this theoretical work is to optimize *ab initio* electronic structures of monohydrates of complexes compound of HCl (C), HNO_3 (N), H_2SO_4 (S) molecules, named CNS ($HCl{\bullet}HNO_3{\bullet}H_2SO_4$) [30]. In this study, it is applied a systematic optimization methodology to reach accurately all possible different optimized geometries for each monohydrate, theirs vibrational modes of frequencies, IR spectra, the wavenumbers of hydrogen bonds, inter-monomeric parameters, electronic and Gibbs free energies, for each optimized candidate geometry whose results will be checked with experimental results. The outcomes will be useful for experimentalist researchers of a vast range of science fields.

2. Methodology

The goal of this work is to obtain the different monohydrates of complexes previously optimized, compound with HCl, HNO_3 and H_2SO_4, named CNS, where HNO_3 was moiety placed in all aggregates of its group [30]. Moreover, to know the shifting in the IR spectrum for each hydrogen bonding obtained on each monohydrates electronic structure. The geometry optimizations have been developed with DFT method alongside the B3LYP hybrid method and Dunning basis set, being aug-cc-pVTZ the primary basis set used —following up previous outcomes—, to reach the optimization of all electronic structures for each one of seven CNS aggregates groups assessed.

2.1. New optimization procedure of electronic structures of monohydrates

To achieve the different optimized electronic structures for each one of CNS aggregates was necessary to follow up on the same systematic methodology of optimization for each of them. In order to obtain largest number of possible hydrogen bond for each CSN complex, the H_2O molecule has been situated systematically around them to favor the creation of the hydrogen bonds, taking into account the free electron pairs on each atom involved, on every CSN-aggregate optimized.

2.2. Nomenclature

The seven CNS-aggregates [30] are here named CNS−*K*, where the −*K* specify which of seven CNS-aggregates pre-optimized is referred, i.e. –*K* = –*1*, –*2* … –*7*. The CNS–*1* is associated to CNS-a (see Ref. [30]), where the CNS-*b*, *-c*, *-d*, *-e*, *-f* and *-g* have been nomenclated as CNS–*2*, CNS–*3* … and CNS–*7*, that are belonging to the remaining CNS-structures. The monohydrates of each CNS-K aggregate have been symbolized with the acronym CNS−K+$1W_i$. Where the symbol (+1W) represents one H_2O molecule added on each one of CNS–*K* aggregate, and *i* denotes the H_2O position around of the CNS–*K* complex in study, i.e. the acronym (+$1W_{\mathbf{i}}$) means that one H_2O molecule is added on *i* position on each of one of CNS–*K* aggregate. The initial *i* position for H_2O molecule was determined on global minimum CNS–*1* electronic structure —CNS-a in ref. 30—, being the eight H_2O positions nomenclated *i* = *a, b, c, d, e, f, g,* and *h,* following up this nomenclature over all CNS-*K* aggregates. Fig. 1 shows the global minimum CNS-*1* aggregate in which the eight H_2O positions (+$1W_i$) are specified over its optimized geometry, being these *i* positions the position-references to carry out the geometry optimizations for remaining CNS-*K* +$1W_i$ monohydrates.

In Fig. 1, shows CNS-*1* complex, being the oxygen atoms colored in red, the protons in grey, the nitrogen atom in blue, the sulfur atom in yellow and the chlorine atom in green. The intermonomeric distances are shown in dashed blue lines. The *i* positions of H_2O molecule (+1W*i*) have been chosen in favorable positions to create the largest number of possible hydrogen bonds between H_2O molecule and oxygen atoms of the monomers in the CNS-K complexes, like mentioned previously.

2.3. Heterogeneous nucleation kinetic reactions

The heterogeneous nucleation kinetic reactions of the monohydrates of CNS−*K* aggregates follow:

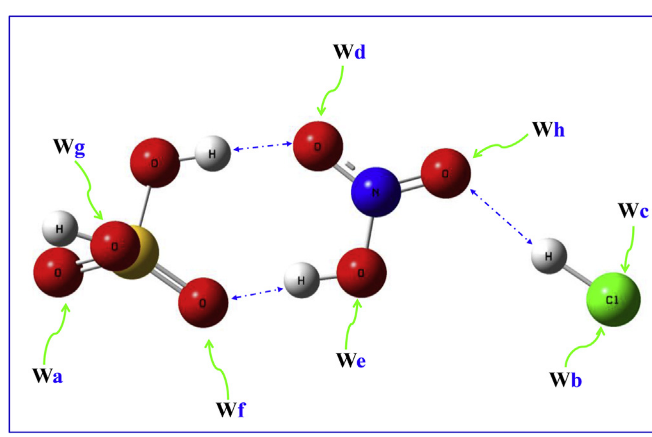

Fig. 1. It illustrates the more possible hydrogen bonds: O–H···O: (+$1\mathbf{W}_i$) on the global minimum ($HCl{\bullet}HNO_3{\bullet}H_2SO_4$)-a aggregate (CNS-a in Ref. [30]) to optimize the (CNS-*K*+$1W_i$.)-monohydrates.

$$[HCl \cdot HNO_3 \cdot H_2SO_4] - K + [H_2O]_i \rightarrow [HCl \cdot HNO_3 \cdot H_2SO_4] - K + 1W_i$$
$$\text{abridged}: [CNS - K] + 1W_i \rightarrow CNS - K + 1W_i \quad (1)$$

where $K = 1$ to 7 for CNS-K complex, while $i = a$ to h. The thermochemistry of the heterogeneous nucleation kinetic reactions gave the relative Gibbs free energy of nucleation of all ($\Delta G_{CNS\text{-}K+1Wi}$)-monohydrates, being the difference between the energy of K-monohydrate and the sum of energy of isolated *monomers*. The relative Gibbs free energy of ($\Delta G_{CNS\text{-}K+1Wi}$)-monohydrates has the expression:

$$\Delta G_{CNS-K+1Wi} = [(E + ZPE) + H - TS]_{k-monohydrate} - \sum[(E + ZPE) + H - TS]_{monomers} \quad (2)$$

where the *K*-monohydrate is the (CNS-*K* $+1W_i$)-monohydrate optimized, being the *monomers* the HCl, HNO_3, H_2SO_4 and H_2O isolated molecules. In equation (2), the *E* is the electronic energy at 0 K; *ZPE* is the zero point energy; *H* is the enthalpy considering the thermal contributions from translational, vibrational and rotational motions; and *S* is the entropy contributions from these motions. The Gibbs free energies have been carried out at 298.15 K degrees of temperature (T) in all geometry optimizations.

On the one hand, the relative Gibbs free energies of nucleation reactions ($\Delta G'_{CNS\text{-}K+1Wi}$) was obtained for each K-monohydrate from *K-reactants*. The relative free energies of nucleation reactions ($\Delta G'_{CNS\text{-}K+1Wi}$) equation follows:

$$\Delta G'_{CNS-K+1Wi} = [(E + ZPE) + H - TS]_{k-monohydrate} - \sum[(E + ZPE) + H - TS]_{k-reactants} \quad (3)$$

where the *K-reactants* are considered the (CNS-*K*)-complexes joint to the ($1W_i$)-H_2O molecule added, that are subtracted to the Gibbs free energy of the k-monohydrate giving the different values of the relative Gibbs free energy $\Delta G'_{CNS-K+1Wi}$ for each CNS-*K* complex evaluated, from $K = 1$ to 7, and $i = a$ to h.

On the other hand, the relative Gibbs free energies of nucleation reactions ($\Delta G''_{CNS\text{-}K+1Wi}$), give the value subtracting the energy from each K-monohydrate regarding (CNS-1) as global minimum complex of the CNS-*K* group, which has the expression:

$$\Delta G''_{CNS-K+1Wi} = \sum[(E + ZPE) + H - TS]_{k-monohydrate} - \sum[(E + ZPE) + H - TS]_{CNS-1+H_2O} \quad (4)$$

where the global minimum CNS-*1* complex and H_2O molecule are considered as reactants. In equations (3) and (4), the E, ZPE, H, S and T were considered with the same concepts and values that in eq. (2).

Moreover, in order to be able to compare the relative stability of (CNS-*K* $+1W_i$)-monohydrates reached, the relative Gibbs free energies of nucleation reaction $\Delta(\Delta G')$ have been obtained regarding the global minimum monohydrate CNS-*1*$+1W_a$. The equation of relative stability $\Delta(\Delta G')$ is:

$$\Delta(\Delta G') = \Delta\left[\Delta G'_{CNS-K+1Wi} - \Delta G'_{global-minCNS-1+1Wa}\right] \quad (5)$$

where $\Delta G'_{CNS-K+1Wi}$ corresponds to the relative Gibbs free energy for each K-monohydrate optimized and $\Delta G'_{global-minCNS-1+1Wa}$ is the value of the relative Gibbs free energy of the global minimum monohydrate CNS-*1*$+1W_a$.

2.4. Computational methodology

Gaussian 09-program suite [37] has been used for all geometry optimizations of monohydrates of the CNS–*K* aggregates group. Previously, the CNS–*K* molecular aggregates were calculated and calibrated regarding experimental and theoretical data [30]. The ground-state of electronic structures of (CNS-*K*$+1W_i$)-monohydrates have been carried out within DFT method using B3LYP (Becke three parameters exchange potential and Lee-Yang-Parr correlation functional) [38,39], and aug-cc-pVTZ (5d, 7f) Dunning's basis set [40–42] at high level of theory. For the optimization of (CNS-*K*$+1W_i$)-monohydrates have been required one, two, even six Z-matrixes as intermediary procedure to reach theirs global minima. Theirs ground-state geometries have been optimized at 0 K of temperature, taking into account their 652 basis functions for each CNS-*K*$+1W_i$ monohydrate, which all have C1 symmetry. At 298.15 K of temperature has been calculated the thermochemistry. The Gibbs free energies have been calculated at same high level of theory than electronic energies of all CNS-*K*$+1W_i$ monohydrates.

Notice that, on the one hand, the B3LYP level of theory was confirmed like appropriate hybrid method to reach HB [43]; on the other hand, Givan et al. suggest that the aug-cc-pVTZ basis set provides sufficient and reasonable description for the complexes than the aug-cc-pVQZ basis set, saving computational efforts [44]. For this reason, the B3LYP method and aug-cc-pVTZ have been selected, that had been previously checked regarding CCSD(T) and PW91 methods [30].

3. Results and discussion

The optimizations of candidate (CNS-K$+1W_i$)-monohydrates structures have yielded forty-eight optimized geometries, after the analysis of electronic energies for nucleation kinetic reactions (Eq. (1)), being fifty-six the initial candidate geometries to optimize (See Fig. S1 – S7 in SM). The assessment of the electronic energies (See Table S1 in SM) reveals that (CNS-*1*$+1W$*a*)-monohydrate is the most stable monohydrate reached, shown in Fig. 2. The (CNS-*1*$+1W$*a*)-monohydrate gave the global minimum structure regarding remaining (CSN-*K*$+1W_i$)-monohydrates geometries achieved.

The systematic geometry optimizations of CNS-*K*$+1W_i$ structures show that only thirty-two monohydrate are different in geometry from forty-eight monohydrates previously optimized, i.e. only thirty-two monohydrates converge with different structure over fifty-six initial geometries of CNS-*K*$+1W_i$ (See Table S1 in SM). The monohydrates CNS-*K*$+1W$*a* converged at first step of optimization are $K = 1, 5, 3$ and 2. The remaining geometries needing at least two optimization steps, being the CNS-*4*$+1W_i$, which requires until six Z-matrixes to converge, and only reaches three geometries. The CNS-*1*$+1W$*a* structure (Fig. 2) shows four inter-monomeric HBs, keeping its hexagonal ring among HNO_3 and H_2SO_4 monomers. One proton of the HNO_3 and one other of H_2SO_4 develop a hexagonal ring in the electronic structure of CNS-*1*$+1W$*a*. The proton donated by HNO_3 towards H_2SO_4 gives the d(OH···O) distance: 1.65 Å, whereas the H_2SO_4 proton transferred to HNO_3 affords the distance d(OH···O) = 1.80 Å. This latest both distances maintain the hexagonal ring between HNO_3 and H_2SO_4 monomers. The inter-monomeric distance between H_2O molecule and closer proton of H_2SO_4 gives d(OH···O) = 1.635 Å. The latest distance is in accordance with d(OH···O) = 1.645 Å obtained by Fiacco et al. [16]. The bond distance d(OH···O) = 2.163 Å corresponds to the proton of HCl transferred to HNO_3 monomer that is in agreement with the distance d(OH···O) = 2.163 Å obtained by Gómez et al. shown on their N2A-1C3W structure in Ref. [27]. The structure of (CNS-

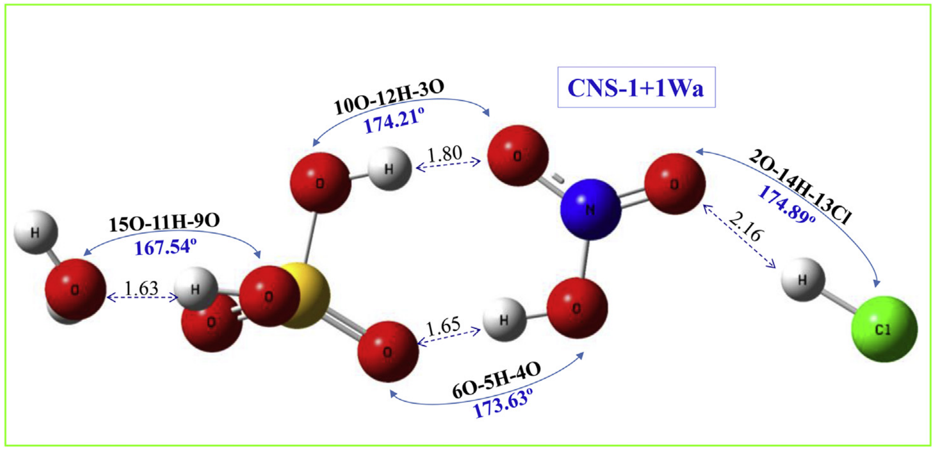

Fig. 2. The (CNS-*1*+1W*a*)-monohydrate is the relative global minimum among all monohydrates optimized, where CNS-complex was K = 1 and the favorable H_2O position was *i* = a. The intermonomeric distances are: (S)-O—H···O-$(H)_2$ gave 1.63 Å, the d(N)-O—H···O-(S) gave 1.65 Å, the d(S)-O—H···O-(N) is 1.80 Å and the d(N)-O···H (Cl) gave 2.16 Å. This geometry was optimized at B3LYP/aug-cc-pVTZ method and basis set at high level of theory. Its electronic energy is $E_h = -1518.676297$ Hartree. The hexagonal ring follows-up in the monohydrate.

Table 1
Displays the relative electronic energies (ΔE) for all (CNS-*K*+1W$_i$)-monohydrates regarding to (CNS-*1*+1W*a*)-monohydrate as the relative global minimum.

Monohydrates of CNS-*K*+1W$_i$	-*i*	ΔE (Kcal/mol)	Shape
CNS-***1***+1W$_i$	*a*	0.00	hexagonal ring
CNS-***5***+1W$_i$	*f*	0.18	hexagonal ring
CNS-***3***+1W$_i$	*f*	0.31	hexagonal ring
CNS-***2***+1W$_i$	*f*	0.47	pentagonal ring
CNS-***4***+1W$_i$	*b* = *c* = *h*	0.61	hexagonal ring
CNS-***6***+1W$_i$	*c*	1.64	irregular ring
CNS-***7***+1W$_i$	*a*	3.89	irregular ring

$E_h = -1518.676297$ Hartree is the electronic energy the global minimum (CNS-*1*+1W*a*)-monohydrate. The ΔE is the increase regarding the energy of CNS-*1*+1W*a*. The Zero Energy Potential Correction (ZEPC) was add in all electronic energies obtained.

1+1Wa)-monohydrate generates angles nearby to straight angle like they are the values 173.63° and 174.21° that correspond to the angles between oxygen atoms of HNO_3 and H_2SO_4 acids which maintain the hexagonal ring in the monohydrate. The HCl molecule and oxygen atom of HNO_3 creates the angle value 174.89°. The (S)-OH proton of H_2SO_4 and H_2O molecule gives the angle value 167.54° that is in consonance with experimental angle datum: 165.4° [16]. The inter-monomeric parameters have been exhibited over all different (CNS-*K*+1W$_i$)-monohydrates reached in this work (See Fig. S8 − S14 in SM). The (CNS-*K*+1W$_i$)-monohydrates gives four HB, even in the monohydrates lower stable energetically which develop an irregular structure. The (CNS-*1*+1W*a*)-monohydrate gives the electronic energy value $E_h = -1518.676297$ Hartree. It has the global relative electronic structure assigned the ΔE = 0.0 kcal mol^{-1}. Notice that the H_2O, HNO_3, H_2SO_4 and HCl molecules develop a linear structure on its monohydrate maintaining the hexagonal ring between HNO_3 and H_2SO_4 like on its trimer. The (CNS-*1*+1Wd)-monohydrate produces a quasi-pentagonal ring on its structure which has ΔE = 0.96 kcal mol^{-1} being the second relative stable monohydrate on the same (CNS-*1*+1W$_i$)-monohydrate group (See Fig. S1-B in SM). All the ground-state structures of the remaining (CNS-*K*+1W$_i$)-monohydrates can see in SM (Fig. S1 − S7).

Table 1 shows the global relative electronic energies for each group of (CNS-*K*+1W$_i$)-monohydrates optimized with respect to (CNS-*1*+1W*a*)-monohydrate as the global minimum among all monohydrates optimized in this work, which has $E_h = -1518.676297$ Hartree of electronic energy, as said prior, and the kind of rings developed on each structure.

The analysis of monohydrates geometries permits us to assess the different structures achieved regarding to the monohydrates candidates. Notice that, the geometry of (CNS-*5*+1W*f*)-monohydrate has 0.18 kcal mol^{-1} of electronic energy which converges with the same structure as (CNS-*5*+1W*e*)-monohydrate which has 0.19 kcal mol^{-1} of relative electronic energy (See Figs. S5−A and S5−B in SM). The monomers of (CNS-*5*+1W*f*)-monohydrate maintain the hexagonal ring between HNO_3 and H_2SO_4, placing the HCl and H_2O molecules below the X-axis (See Figs. S5A and S5B in SM). The CNS-*3*+1W*f* monohydrate structure has 0.31 kcal mol^{-1} of relative electronic energy preserving too its hexagonal ring (See Fig. S3A in SM). The CNS-*2*+1W*f* monohydrate creates a quasi-pentagonal ring —like others optimized monohydrates in its group—, being 0.47 kcal mol^{-1}the value of relative electronic energy, in which the HCl is placing above X-axis (See Fig. S2A in SM). The optimization of (CNS-*4*+1W*i*)-monohydrate group, produces only three monohydrates structures *i* = *b*, *c* and *h*, all of which develop the same geometry, maintaining the hexagonal ring between the HNO_3 and H_2SO_4, and placing HCl and H_2O molecules below the X-axis. These local minimum (CNS-*4*+1W$_i$)-monohydrate has ΔE = 0.61 kcal mol^{-1} of relative electronic energy (See Fig. S4 in SM). On the (CNS-*6*+1W$_i$)-monohydrate group (See Fig. S6 in SM), and CNS-7+1Wi monohydrates group (See Fig. S7 in SM) the rings disappear. The (CNS-*6*+1W$_c$) and (CNS-*7*+1W$_a$)-monohydrates gave higher relative electronic energy values as 1.64 and 3.89 kcal mol^{-1} respectively. The *cis* protons of H_2SO_4 molecule offer unstable structures on *i* = *a, b, c, g* positions on (CNS-5+1Wi)-monohydrate, and for (CNS-*6*+1W$_i$)-monohydrates on the places *i* = *c, d, e*.

The (CNS-*1*+1Wd)-monohydrate given the value 0.96 kcal mol^{-1} for the relative electronic energy — second relative energy in its group (See Tables S1−B in SM)— being lower stable than others local minima of (CNS-*K*+1W$_i$)-monohydrates, where *K* = *5, 3, 2* and *4*. This energetic behavior is due possibly to the creation of a pentagonal ring in its structure. The development of hexagonal ring seems to predominate in (CNS-*K*+1W$_i$)-monohydrates. When the HNO_3 and H_2SO_4 molecules share only one *cis* proton, the monohydrates generate irregular rings, which possess higher electronic energies. The geometrical structures for all (CNS-*K*+1W$_i$)-monohydrates can see on Table S1 in SM. The relative energy increases (ΔE) for each group of (CNS-*K*+1W$_i$)-monohydrates regarding 1W$_i$ position can see in Table S2 in SM. The W$_f$

position seems to be most stable for the monohydrates *K* = *2, 3* and *5*. Focusing on the global minimum CNS-*1*+1W*a* monohydrate, its proton transference is produced by *trans* protons of H_2SO_4 molecule, one proton manages to H_2O molecule, other one towards HNO_3 molecule, being the proton of HCl transferred to external oxygen atom of HNO_3. When the H_2SO_4 protons are in *trans* position produce most stable (CNS-*K*+1W$_i$)-monohydrates. However, the *cis* protons of H_2SO_4, produce only the (CNS-*4*+1 W$_h$)-monohydrate, and (CNS-6+1W$_i$)-monohydrates group generate two stable monohydrates *i* = *c* and *e*, from six candidate geometries. When H_2SO_4 molecule transfers only one proton, the (CNS-*K*+1W$_i$)-monohydrates shown lower stability. On the one hand, the HNO_3 molecule transfers its proton to H_2SO_4 molecule mainly; on the other hand, the HCl molecule transfers always its proton towards closer neighboring oxygen atom.

The IR spectra have been predicted for each one of (CNS-*K*+1W$_i$)-monohydrates, taking into account their 45 degrees of freedom. All real harmonic vibrational frequencies have been calculated at B3LYP/aug-cc-pVTZ of high level of theory within DFT method, as mentioned in Methodology. The wavenumbers of HB have been explicit in Table 2 for all (CNS-*K*+1W$_i$)-optimized monohydrates. The IR spectra of (CNS-*K*+1W$_i$)-monohydrates show the wavenumbers of protons transfer for each HB. The shifting for the HB of HCl molecule moves in the range from 2887 cm^{-1} until 2573 cm^{-1}, in agreement with experimental results by Ortega et al. [33]. The displacements range for HB of HNO_3 molecule starts from 3376 cm^{-1} until 2668 cm^{-1}. These latest values are in consonance with 3490–3260 cm^{-1} range for OH stretching modes like Wagner et al. [11] summarized. The wavenumbers of H_2SO_4 protons shift for first proton transferred from 3530 cm^{-1} to 2972 cm^{-1}, and for the second proton transferred from 3577 to 3451 cm^{-1}, in accordance with experimental data [31–36].

Fig. 3 shows the symmetric stretching modes for the global minimum (CNS-*1*+1Wa)-monohydrate over its own IR spectrum. The HB of (CNS-*1*+1W*a*)-monohydrate appears at 3035 cm^{-1} with a strong peak that corresponding to symmetric stretching mode of *trans* proton of H_2SO_4 transferred towards H_2O molecule. The second proton of H_2SO_4 shifts at 3459 cm^{-1} with a medium peak of intensity with symmetric stretching mode, corresponding to proton transfer towards oxygen atom of HNO_3 molecule. The proton transfer of HNO_3 shifts at 3139 cm^{-1} that develop the hexagonal ring with H_2SO_4. The shifting of HNO_3 proton occurs at 1704 cm^{-1} in the (CNS-*1*+1Wa)-monohydrate that is in consonance with the value 1740 cm^{-1} reported by Wagner et al. [11]. The shifting of HCl proton appears at 2858 cm^{-1} showing a weak peak, in consonance with experimental data [33].

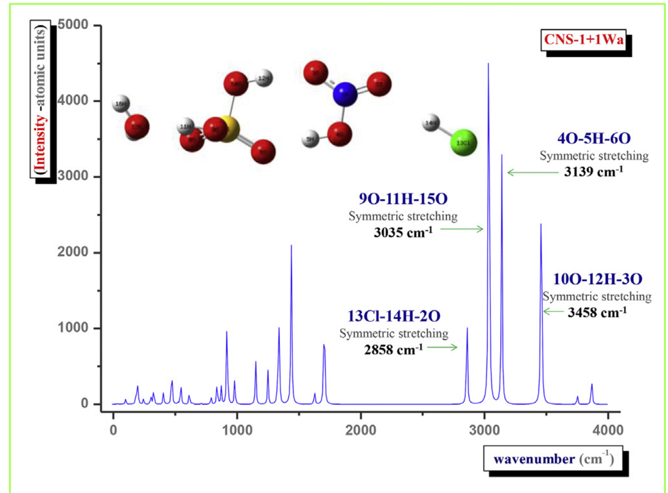

Fig. 3. IR spectrum of CNS-*1*+1W*a* shows the shifts of the four HBs predicted corresponding to vibrational motions of the symmetric stretching modes.

Table 3 exhibits the relative Gibbs free energies for each one of the different (CNS-*K*+1W$_i$)-monohydrate optimized. As mentioned in Methodology, Eq. (2) gives the Gibbs free energy of nucleation reactions (ΔG) from isolated molecules. Eq. (3) provides the Gibbs free energies (ΔG′) of nucleation reaction from *K-reactants* (written in italic in Table 3), for each one of −*K* aggregate addend H_2O molecule in *i* position. Eq. (4) supplies the values (in bold) of Gibbs free energy (ΔG″) for nucleation reactions of monohydrates from initial global minimum trimer (CNS-*1*) addend one H_2O molecule as reactants. Eventually, Eq. (5) affords the relative Gibbs free energies [Δ(ΔG')] for nucleation of CNS-*K*+1W$_i$ monohydrates from the global minimum (CNS-*1*+1W*a*)-monohydrate reached, whose values have been expressed in italic and bold typography in Table 3.

After to apply the systematic optimization methodology over all (CNS-*K*+1W$_i$)-monohydrates, the (CNS-*1*+1W*a*)-monohydrate shows as the most stable monohydrate whose relative Gibbs free energy is Δ(ΔG′) = 0.0 Kcal mol^{-1}, being the remaining relative Gibbs free energies obtained: ΔG = −16.58 Kcal mol^{-1}, ΔG' = −10.90 Kcal mol^{-1} and ΔG" = −10.90 Kcal mol^{-1}. The relative Gibbs free energies values correspond to nucleation reactions from global minimum (CNS-*1*+1W*a*)-monohydrate, from isolated monomers, *K*-reactants and CNS-1 + H_2O, respectively. The (CNS-*1*+1W*a*)-monohydrate considered as global minimum monohydrate, keeping its global minimum position through all (CNS-

Table 2
Wavenumbers of hydrogen bonds (HB) for most stable structures of each (CNS-*K*-1W$_i$)-monohydrate group.

Monohydrate	ΔE (kcal mol^{-1})	Shifting (HB)$_1$	Shifting (HB)$_2$	Shifting (HB)$_3$	Shifting (HB)$_4$
CNS-*1*+1W*a*	0.00	13Cl-14H—2ON 2858 cm^{-1}	4O-5H—6OS 3139 cm^{-1}	9O-11H—15O 3035 cm^{-1}	10O-12H—3ON4 3459 cm^{-1}
CNS-*5*+1W*f*	0.18	13Cl-14H—4ON 2784 cm^{-1}	4O-5H—6OS 2930 cm^{-1}	9O-10H—15OH 2972 cm^{-1}	11O-12H—2OS 3534 cm^{-1}
CNS-*3*+1W*f*	0.31	14Cl-13H—4ON 2887 cm^{-1}	4O-5H—6OS 3137 cm^{-1}	9O-11H—15OH 3031 cm^{-1}	10O-12H—3ON 3454 cm^{-1}
CNS-*2*+1W*f*	0.47	14Cl-13H—3ON 2722 cm^{-1}	4O-5H—6OS 3338 cm^{-1}	9O-11H—15OH 3045 cm^{-1}	10O-12H—14Cl 3451 cm^{-1}
CNS-*4*+1 Wh	0.61	13Cl-14H—3ON 2780 cm^{-1}	4O-5H—8OS 2987 cm^{-1}	9O-10H—15OH 3181 cm^{-1}	11O-12H—2ON 3528 cm^{-1}
CNS-*6*+1W*c*	1.64	14Cl-13H—8OS 2573 cm^{-1}	4O-5H—15OH 2668 cm^{-1}	9O-11H—4ON 3530 cm^{-1}	10O-12H—2ON 3577 cm^{-1}
CNS-*7*+1W*a*	3.89	14Cl-13H—2ON 2722 cm^{-1}	4O-5H—8OS 3376 cm^{-1}	9O-11H—15OH 3025 cm^{-1}	10O-12H—14Cl 3515 cm^{-1}

The (HB)$_1$ corresponds to the HCl proton transferred; (HB)$_2$ is the HNO_3 proton transferred; (HB)$_3$ expresses the first proton transference (H1) of H_2SO_4 and (HB)$_4$ gives the second proton transferred (H2) of H_2SO_4. The wavenumbers have been explicit in cm^{-1}.

Table 3
Relative Gibbs free energies (ΔG, ΔG′ y ΔG″) for all different *ab initio* (CNS-K+1W$_i$)-monohydrates.

Table 3. Relative Gibbs free energies (ΔG, ΔG' y ΔG'') for all different *ab initio* (CNS-*K*+1W$_i$)-monohydrates

Monohydrate CNS(-*K*)	**-1**	**-2**	**-3**	**-4**	**-5**	**-6**	**-7**
position (+W$_{-i}$)	**Δ Gibbs free Energy of nucleation reaction for each CNS-*K*+1W$_i$**						
-a	-16.58 *-10.90* **-10.90** ***0.00***	—	—	—	—	—	-7.82 *-16.95* **-2.14** ***8.77***
-b	—	-14.18 *-10.19* **-8.50** ***2.40***	—	-12.68 *-9.71* **-6.99** ***3.91***	—	—	7.89 *-1.24* **13.57** ***24.47***
-c	—	—	-1.73 *3.40* **3.95** **14.85**	—	—	-10.66 *-13.93* **-4.98** ***5.92***	—
-d	-15.18 *-9.50* **-9.50** ***1.40***	-0.65 *3.34* **5.03** ***15.93***	-14.83 *-9.69* **-9.14** ***1.76***	—	-14.18 *-11.41* **-8.50** ***2.40***	-12.93 *-16.21* **-7.25** ***3.65***	7.13 *-2.00* **12.81** ***23.71***
-e	-1.34 *4.34* **4.34** ***15.24***	-1.58 *2.41* **4.10** ***15.01***	0.29 *5.42* **5.97** ***16.87***	—	-14.07 *-11.30* **-8.39** ***2.51***	-3.80 *-7.08* **1.88** ***12.78***	-1.58 *-10.71* **4.10** ***15.01***
-f	-1.28 *4.40* **4.40** ***15.30***	-14.99 *-11.01* **-9.31** ***1.59***	-16.55 *-11.42* **-10.87** ***0.03***	—	-14.09 *-11.32* **-8.41** ***2.49***	—	-6.50 *-15.63* **-0.82** ***10.09***
-g	-1.00 *4.68* **4.68** ***15.58***	-1.58 *2.41* **4.10** ***15.01***	-16.53 *-11.39* **-10.84** ***0.06***	—	-14.32 *-11.55* **-8.64** ***2.26***	—	—
-h	-1.58 *4.10* **4.10** ***15.01***	-0.74 *3.24* **4.94** ***15.84***	-1.45 *3.68* **4.23** ***15.13***	—	-8.59 *-5.81* **-2.90** ***8.00***	—	-1.58 *-10.71* **4.10** ***15.04***

The sum of Gibbs free energies of isolated *monomers* is −1905982.41 Kcal mol^{-1}; for each –*K* local minimum *reactant* is: *K = 1* (–1905988.09 Kcal mol^{-1}), *K = 2* (–1905986.40 Kcal mol^{-1}), *K* = 3 (–1905987.55 Kcal mol^{-1}), *K = 4* (–1905985.38 Kcal mol^{-1}), *K = 5* (–1905985.19 Kcal mol^{-1}), *K = 6* (–1905979.14 Kcal mol^{-1}), *K = 7* (–1905973.28 Kcal mol^{-1}) from each reactants. The sum of Gibbs free energies from global minimum CNS-*1* and H_2O molecule (*CNS-1+H$_2$O*) as reactants gives –1905988.09 Kcal mol^{-1}. The global minimum monohydrate CNS-*1*+1W*a* has -1905999.00 Kcal mol^{-1} like relative Gibbs free energy. All Gibbs free energies have been carried out at 298.15 K. Results provided in Kcal mol^{-1}. The ΔG (standard), *ΔG'* (in italic), **ΔG''** (in bold) and ***Δ(ΔG')*** (in bold and italic) correspond to increases from monomers, *K-reactants, CNS-1+H$_2$O,* and global minimum (CNS-*1*+1W*a*)-monohydrate.

The sum of Gibbs free energies of isolated *monomers* is -1905982.41 Kcal mol^{-1}; for each $-K$ local minimum *reactant* is: $K=1$ (-1905988.09 Kcal mol^{-1}), $K=2$ (-1905986.40 Kcal mol^{-1}), $K=3$ (-1905987.55 Kcal mol^{-1}), $K=4$ (-1905985.38 Kcal mol^{-1}), $K=5$ (-1905985.19 Kcal mol^{-1}), $K=6$ (-1905979.14 Kcal mol^{-1}), $K=7$ (-1905973.28 Kcal mol^{-1}) from each reactants. The sum of Gibbs free energies from global minimum CNS-*1* and H_2O molecule (*CNS-1+H$_2$O*) as reactants gives -1905988.09 Kcal mol^{-1}. The global minimum monohydrate CNS-*1*+1W*a* has -1905999.00 Kcal mol^{-1} like relative Gibbs free energy. All Gibbs free energies have been carried out at 298.15 K. Results provided in Kcal mol^{-1}. The ΔG (standard), *ΔG′* (in italic), **ΔG''** (in bold) and ***Δ(ΔG′)*** (in bold and italic) correspond to increases from monomers, *K-reactants, CNS-1+H$_2$O,* and global minimum (CNS-*1*+1W*a*)-monohydrate.

K+1W$_i$)-monohydrates. These relative Gibbs free energy values are due to the proton positions of the H_2O molecule which are upward, facing the protons of CNS-3+1W*f* that are positioned downward of X-plane, for instance. The monohydrates CNS-3+1W*f* and CNS-*2*+1W*f* gave Δ(ΔG′) = 0.03 Kcal mol^{-1} and Δ(ΔG′) = 1.59 Kcal mol^{-1} of values for relative Gibbs free energy from global minimum monohydrate. The latest both monohydrates develop a hexagonal ring in their geometries with HNO_3 and H_2SO_4 molecules. It seems the −*f* H_2O position results favorable in several monohydrates reached as can see in Table 3. The remaining relative stable (CNS-K+1W$_i$)-monohydrates also can observe in Table 3. The relative Gibbs free energy values oscillate from 0.0 to 8.77 Kcal mol^{-1} for Δ(ΔG′), (yellow color in Table 3), from −16.58 to −7.82 Kcal mol^{-1} for ΔG, from −16.95 to −9.71 Kcal mol^{-1} for ΔG′, and from −10.90 to −2.14 Kcal mol^{-1} for ΔG''.

The empty boxes with hyphens correspond to the structures of (CNS-K+1W$_i$)-monohydrates optimized that gave equal geometry in the optimization process on the $_{-i}$ positions for −K groups of monohydrates optimized, i.e. the optimized monohydrate structure converges with equal geometry than other structure optimized.

The lower stable monohydrate among (CNS-K+1W$_i$)-monohydrates optimized, corresponds to (CNS-*7*+1W*a*)-monohydrate, whose relative Gibbs free energy is Δ(ΔG′) = 8.77 Kcal mol^{-1} from global minimum (CNS-*1*+1W*a*)- monohydrate. The three unstable monohydrates result: (CNS-*3*+1W*e*), (CNS-*7*+1Wb) and (CNS-*7*+1Wd), being their relative Gibbs free energies (ΔG) from isolated monomers 0.29 Kcal mol^{-1}, 7.89 Kcal mol^{-1} and 7.13 Kcal mol^{-1}, respectively (grey color in Table 3). This thermochemistry behavior is keeping for their remaining Gibbs free energies, ΔG′, ΔG″ and Δ(ΔG′) for these three monohydrates.

This systematic optimization methodology affords thirty-two different structures optimized from fifty-six candidate geometries. These thirty-two electronic structures of (CNS-*K*+1W$_i$)-monohydrates could be consider as possible precursors of some heterogeneous nucleation reactions in PSCs. These (CNS-*K*+1W$_i$)-monohydrates structures, with their hydrogen-bonds have been specified on each one of electronic structure shown, could facilitate to experimental researchers to elucidate some nucleation reactions in PSC that take part in the stratosphere. Besides, these outcomes could be useful for industrial areas, like industrial smog, even catalytic and corrosion processes and reactions in extraterrestrial scenarios.

The initial (CNS-K+1W$_i$)-monohydrates achieved through this systematic optimization methodology have been exhibited at EMN meeting on Computational and Theory, October, 19–14, 2016 Las Vegas, NV, USA.

4. Conclusions

The systematic optimization process have been carried out placing the H_2O molecule on eight positions around of the CNS-*K* group of complexes to create all Z-matrixes of the (CNS-*K*+1W$_i$)-monohydrates. After to apply this systematic optimization method to achieve the electronic structures of (CNS-K+1W$_i$)-monohydrates, it can conclude the following:

a) Thirty-two different optimized electronic structures of (CNS-K+1W$_i$)-monohydrates have been obtained from fifty-six initial candidate geometries. These findings explain the chemical, microphysical, and dynamical atmospheric processes that involve the HCl [45], even these geometries may improve the understanding of the various types of particles within a single cloud [46]. Moreover, these results are in consonance with the coexistence of several hydrates of HCl, HNO_3 and H_2SO_4 mixtures [47–49]. These monohydrates can be atmospheric precursors of heterogeneous nucleation reactions.
b) The global minimum is the (CNS-*K*+1W*a*)-monohydrate, whose electronic energy gave −1518.676297 Hartree, being *-a*, the favorable placement for the H_2O molecule. As well as, the *-f* position is propitious to place H_2O molecule between different (CNS-K+1W$_i$)-monohydrates optimized. The unfavorable H_2O positions are *-c*, *-g* and *-h*.
c) The relative electronic energy (ΔE) range for (CNS-*K*+1W$_i$)-monohydrates oscillates from 0.0 Kcal mol^{-1} of the (CNS-*1*+1Wa)-global minimum, until 3.89 Kcal mol^{-1} belonging to (CNS-*7*+1W*a*)-monohydrate structure.
d) The IR spectra have been predicted for the thirty-two electronic structures of (CNS-K+1W$_i$)-monohydrates. The O-H stretching modes are in agreement with experimental results [19,20]. The HBs of (CNS-*K*+1W$_i$)-monohydrates shift in the following ranges: from 2573 to 2878 cm^{-1} for the proton transferred by HCl; from 2668 to 3376 cm^{-1} for the proton transferred by HNO_3; finally, from 2972 to 3530 cm^{-1} and 3451–3577 cm^{-1} for the first and second proton transferred by H_2SO_4. The HBs of the global minimum (CNS-*1*+1W*a*)-monohydrate shift at 2858, 3035, 3139 and 3458 cm^{-1} in its IR spectrum, corresponding to the symmetric stretching modes of proton transferred by HCl, to first proton of the H_2SO_4, to proton of HNO_3, and the second proton transferred of H_2SO_4, respectively.
e) The protonic transference promotes the hexagonal ring between H_2SO_4, and HNO_3 molecules on the global minimum (CNS-*K*+1W*a*)-monohydrate. Moreover, the *trans* protons of H_2SO_4 create easily relative stable (CNS-*K*+1W$_i$)-monohydrates. The *trans* or *cis* proton transfer of H_2SO_4 molecule, generates the hexagonal, linear, irregular or aspherical structures, in agreement with Wagner et al. [11].
f) The relative Gibbs free energies calculated from isolated monomers (ΔG), from each *K*-reactants (ΔG′), from CNS-*1* + H_2O (ΔG″), and from global minimum of (CNS-*K*+1W$_i$)-monohydrates [Δ(ΔG′)], show (CNS-*K*+1W*a*)-monohydrate as most relative stable monohydrate, with a relative Gibbs free energy as −1905999.0 Kcal mol^{-1}. The ranges of the different Gibbs free energies oscillate from −16.6 for (CNS-*1*+1W*a*) to −7.8 Kcal mol^{-1} for (CNS-*7*+1W*a*)-monohydrate; from −10.9 to −16.9 Kcal mol^{-1}; from −10.9 until −2.1 Kcal mol^{-1}, and from 0.0 to 8.8 Kcal mol^{-1} for the Gibbs free energies (ΔG), (ΔG′), (ΔG″) and [Δ(ΔG′)] respectively, and for the same monohydrates. The relative stability seems to be related with the hexagon ring constructed by HNO_3 and H_2SO_4 molecules and the protons transferred among them.
g) Applying this systematic optimization method guarantees to reach all different *ab initio* optimized geometries in order to obtain the major quantity of different (CNS-*K*+1W$_i$)-monohydrates.
h) *Ab initio* optimizations of HCl-H_2SO_4-HNO_3 monohydrates structures will be generate from CSN aggregates group.
i) Research is needed to understand exactly the mechanism of such processes in the future: environmental pollution [50–52], corrosion of metals and ceramics [53–57], reactions with organic compounds [58,59], and catalysis reactions [60].

Acknowledgements

The author thanks the computational support of Prof. Dr. M. Paniagua, and Dr. Rafael López in the Applied Physical Chemistry Department at Autonomous University of Madrid

Appendix A. Supplementary data

Supplementary data to this article can be found online at https://doi.org/10.1016/j.jmgm.2018.10.025.

References

[1] P. Hamill, R.P. Turco, O.B. Toon, On the growth of Nitric and Sulfuric acid aerosols particles under stratospheric conditions, J. Atmos. Chem. 7 (1998) 287–315.
[2] T. Ohtake, Freezing points of H_2SO_4 aqueous solutions and formation of stratospheric ice clouds, Tellus 45B (1993) 138–144.
[3] G. Tóth, Quantum Chemical study of the different forms of nitric acid monohydrate, J. Phys. Chem. 101 (1997) 8871–8876.
[4] G. Gleistmann, R. Zellner, The aerosol dynamics of H_2O–H_2SO_4–HNO_3 mixtures in aircraft wakes. A modeling study, Phys. Chem. Chem. Phys. 1 (1999) 5503–5509.
[5] H. Kobara, A. Wakisaka, K. Takeuchi, T. Ibusuki, Cluster structures in aqueous HNO_3 and H_2SO_4 solutions: in relation with equivalent conductivity, J. Phys. Chem. 106 (2002) 4779–4783.
[6] R.A. Cox, M.A. Fernández, A. Symington, M. Ullerstam, J.P. Abbatt, A kinetic model for uptake of HNO_3 and HCl on ice a coated wall flow system, Phys. Chem. Chem. Phys. 7 (2005) 3434–3442.
[7] D. Hanson, K. Mauersberguer, Laboratory studies of nitric acid trihydrate: implications for the south polar stratosphere, Geophys. Res. Lett. 15 (1998) 855–858.
[8] N. Barton, B. Rowland, O. Deblin, Infrared spectra of large acid hydrate clusters: formation conditions of submicrom particles of HNO_3•$2H_2O$ and HNO_3•$3H_2O$, J. Phys. Chem. 97 (1993) 5848–5851.
[9] C. Voigt, J. Schreiner, A. Kohlmann, P. Zink, K. Mauersberger, N. Larsen, T. Deshler, C. Kröger, J. Rosen, A. Adriani, F. Cairo, G. di Donfrancesco, M. Viterbini, J. Ovarlez, H. Ovarlez, C. David, A. Dörnbrack, Nitric acid trihydrate (NAT) in polar stratospheric clouds, Science 290 (2000) 1756–1758.
[10] C. Voigt, H. Schlager, B.P. Luo, A. Dörnbrack, P. Roiger, P. Stock, J. Curtius, H. Vössing, S. Borrmann, S. Davies, P. Konopka, C. Schiller, G. Shur, T. Peter,

Nitric acid trihydrate (NAT) formation at low NAT supersaturation in polar stratospheric clouds (PSCs), Atmos. Chem. Phys. 5 (2005) 1371–1380.

[11] R. Wagner, O. Möhler, H. Saathoff, O. Stetzer, U. Schurath, Infrared spectrum of nitric acid dihydrate: influence of particle shape, Phys. Chem. 109 (2005) 2572–2581.

[12] M. Walker, C.A. Morrison, D.R. Allan, Nitric acid monohydrates at high pressure: an experimental and computational study, Phys. Rev. B 72 (224106–1) (2005) 22106–22109.

[13] O. Möhler, H. Bunz, O. Stetzer, Homogenous nucleation rates of nitric acid dihydrate (NAD) at simulated stratospheric conditions- Part II: modeling, Atmos. Chem. Phys. Discuss. 6 (2006) 2119–2149.

[14] S.T. Martin, D. Salcedo, L.R. Molina, M.J. Molina, Deliquescence of sulfuric acid tetrahydrate following volcanic eruptions or denitrification, Geophys. Res. Lett. 25 (1998) 31–34.

[15] L.T. Iraci, T.J. Fortin, A.M. Tolbert, Dissolution of sulfuric acid tetrahydrate at low temperatures and subsequent growth of nitric acid trihydrate, J. Geophys. Res. 103 (1998) 8491–8498.

[16] D.L. Fiacco, S.W. Hunt, K.R. Leopold KR, Microwave investigation of sulfuric acid Monohydrate, J. Am. Chem. Soc. 124 (2002) 4504–4511.

[17] T. Koop, H.P. Ng, L.T. Molina, M.J. Molina, A new optical technique to study aerosol phase transitions: the nucleation of ice from H_2SO_4 aerosols, J. Phys. Chem. 102 (1998) 8924–8931.

[18] Y. Miller, G.M. Chaban, R.B. Gerber, Ab initio vibrational calculations for H_2SO_4 and H_2SO_4•H_2O: spectroscopy and the nature of the anharmonic couplings, J. Phys. Chem. 109 (2005) 6565–6574.

[19] A.R. Bandy, J. Ianni, Study of the hydrates of H_2SO_4, J. Phys. Chem. 102 (1998) 6533–6539.

[20] P. Räisänen, A. Bogdan, K. Sassen, M. Kulmala, M.J. Molina, Impact of H_2SO_4/H_2O coating and ice crystal size on radiative properties of sub-visible cirrus, Atmos. Chem. Phys. 6 (2006) 4659–4667.

[21] B. Luo, U.K. Krieger, T. Peter, Densities and refractive indices of H_2SO_4/HNO_3/H_2O solutions to stratospheric temperatures, Geophys. Res. Lett. 23 (1996) 3707–3710.

[22] P. Beichert, O. Schrems, Complexes of sulfuric acid with hydrogen chloride, water, nitric acid, chlorine nitrate, and hydrogen peroxide: ab initio investigation, J. Phys. Chem. 102 (1998) 10540–10544.

[23] T. Koop, H.P. Ng, L.T. Molina, M.J. Molina, A new optical technique to study aerosol phase transitions: the nucleation of ice from H_2SO_4 aerosols, J. Phys. Chem. 102 (1998) 8924–8931.

[24] I. Napari, M. Kulmala, H. Vehkamäki, Ternary nucleation of inorganic acids, ammonia, and water, J. Chem. Phys. 117 (2002) 8418–8425.

[25] T. Loerting, A.F. Voegele, C.S. Tautermann, K.R. Liedl, L.T. Molina, M.J. Molina, Modeling the heterogeneous reaction probability for chlorine nitrate hydrolysis on ice, J. Geophys. Res. 111 (2006) D14307.

[26] J. Zhao, N.P. Levitt, R. Zhang, J. Chen, Heterogeneous reactions of methylglyoxal for secondary organic aerosol formation, Environ. Sci. Technol. 40 (2006) 7682–7687.

[27] P.C. Gómez, O. Gálvez, R. Escribano, Theoretical study of atmospheric clusters: HNO_3-HCl-H_2O, Phys. Chem. Chem. Phys. 11 (2009) 9710–9719.

[28] A. Grossel, N. Huret, V. Catoire, G. Berthet, J.B. Renard, C. Robert, B. Gaubicher, In situ balloon-borne measurements of HNO_3 and HCl stratospheric vertical profiles influenced by polar stratospheric cloud formation during the 2005–2006 Arctic winter, J. Geophys. Res. 15 (2010) 1984–2012.

[29] F.M. Balci, N. Uras-Aytemiz, P.C. Gómez, R. Escribano, Proton transfer and autoionization in HNO_3•HCl•(H_2O)n particles, Phys. Chem. Chem. Phys. 13 (2011), 18145 –1815.

[30] M. Verdes, M. Paniagua, Quantum chemical study of atmospheric aggregates: HCl•HNO_3•H_2SO_4, J. Mol. Model. 20 (2014) 2232–2251, https://doi.org/10.1007/s00894-014-2232-6.

[31] B.S. Adult, G.C. Pimentel, Infrared spectrum of the water-hydrochloric acid complex in solid nitrogen, J. Phys. Chem. 77 (1) (1973) 57–61.

[32] J.P. Devlin, N. Uras, J. Sadlej, V. Buch, Discrete stages in the solvation and ionization of hydrogen chloride absorbed on ice particles, Nature 417 (2002) 269–271.

[33] I.K. Ortega, R. Escribano, V.J. Herrero, B. Maté, M.A. Moreno, Exposure of nitric acid trihydrate crystals to HCl: a spectroscopic study, J. Geophys. Res. 111 (2006) D132006 (References therein).

[34] H. Yang, B.J. Finlayson-Pitts, Infrared spectroscopic studies of binary solutions of nitric acid and water and ternary solutions of nitric acid, sulfuric acid, and water at room temperature: evidence for molecular nitric acid at the surface, J. Phys. Chem. 105 (2001) 1890–1896.

[35] M. Walker, C.A. Morrison, D.R. Allan, Nitric acid monohydrates at high pressure: an experimental and computational study, Phys. Rev. B 72 (2005) 224106.

[36] S. Griessbach, L. Hoffmann, R. Spang, M. von Hobe, R. Müller, M. Riese, Infrared limb emission measurements of aerosol in the troposphere and stratosphere, Atmos. Meas. Tech. 9 (2016) 4399–4423.

[37] M.J. Frisch, G.W. Trucks, H.B. Schlegel, G.E. Scuseria, M.A. Robb, J.R. Cheeseman, G. Scalmani, V. Barone, B. Mennucci, G.A. Petersson, H. Nakatsuji, M. Caricato, X. Li, H.P. Hratchian, A.F. Izmaylov, J. Bloino, G. Zheng, J.L. Sonnenberg, M. Hada, M. Ehara, K. Toyota, R. Fukuda, J. Hasegawa, M. Ishida, T. Nakajima, Y. Honda, O. Kitao, H. Nakai, T. Vreven, J.A. Montgomery Jr., J.E. Peralta, F. Ogliaro, M. Bearpark, J.J. Heyd, E. Brothers, K.N. Kudin, V.N. Staroverov, R. Kobayashi, J. Normand, K. Raghavachari, A. Rendell, J.C. Burant, S.S. Iyengar, J. Tomasi, M. Cossi, N. Rega, J.M. Millam, M. Klene, J.E. Knox, J.B. Cross, V. Bakken, C. Adamo, J. Jaramillo, R. Gomperts, R.E. Stratmann, O. Yazyev, A.J. Austin, R. Cammi, C. Pomelli, J.W. Ochterski, R.L. Martin, K. Morokuma, V.G. Zakrzewski, G.A. Voth, P. Salvador, J.J. Dannenberg, S. Dapprich, A.D. Daniels, O. Farkas, J.B. Foresman, J.V. Ortiz, J. Cioslowski, D.J. Fox, Gaussian 09, Revision A.02, Gaussian, Inc., Wallingford CT, 2009.

[38] A.D. Becke, Density-functional thermochemistry. III. The role of exact exchange, J. Chem. Phys. 98 (1993) 5648–5652.

[39] C.T. Lee, W.T. Yang, R.G. Parr, Development of the colle-salvetti correlation-energy formula into a functional of the electron-density, Phys. Rev. B 37 (1998) 785–789.

[40] T.F. Dunning Jr., Gaussian basis sets for use in correlated molecular calculations. I. The atoms boron through neon and hydrogen, J. Chem. Phys. 90 (1989) 1007–1023.

[41] R.A. Kendall, T.H. Dunning Jr., R.J. Harrison, Electron affinities of the first-row atoms revisited. Systematic basis sets and wave functions, J. Chem. Phys. 96 (1992) 6796–6806.

[42] D.E. Woon, T.H. Dunning Jr., Gaussian basis sets for use in correlated molecular calculations. III. The atoms aluminum through argon, J. Chem. Phys. 98 (1993) 1358–1371.

[43] A.D. Rabuck, G.E. Scuseria, Performance of recently developed kinetic energy density functionals for the calculation of hydrogen binding strengths and hydrogen-bonded structures, Theor. Chem. Acc. 104 (2000) 439–444.

[44] A. Givan, A. Loewenschuss, C.J. Nielsen, Infrared spectra and ab initio calculations of the matrix isolated $(CO_2)\cdot(H_2SO_4)$ and $(CO_2)\cdot(SO_3)$ complexes, J. Mol. Struct. 604 (2002) 147–157.

[45] M. Pitts, L. Poole, CALIPSO observations of PSCs and cirrus during the 2015-2016 artic winter, Geophys. Res. Abstr. 18 (2016). EGU2016–3011.

[46] O.B. Toon, A. Tabazadeh, E.V. Browell, J. Jordan, Analysis of lidar observations of Artic polar stratospheric clouds during January 1989, J. Geophys. Res. 105 (2000) 20589–20615.

[47] P.J. Wooldridge, R. Zhang, M.J. Molina, Phase equilibria of H_2SO_4, HNO_3 and HCl hydrates and the composition of polar stratospheric clouds, J. Geophys. Res. 100 (1995) 1389–1396.

[48] D.R. Hanson, Reaction of $ClONO_2$ with H_2O and HCl in sulfuric acid and HNO_3/H_2SO_4/H_2O mixtures, J. Phys. Chem. 102 (1998) 4794–4807.

[49] Q. Wang, J. Zhao, W. Du, G. Ana, Z. Wang, L. Sun, Y. Wang, F. Zhang, Z. Li, X. Ye, Y. Sun, Characterization of submicron aerosols at suburban site in central China, Atmos. Environ. 131 (2016) 115–123.

[50] S.L. Tian, X.J. Liu, Y.P. Pan, Y.B. Zhou, W. Xu, Y.S. Wang, Observations of reactive nitrogen and sulfur compounds during haze episodes using a denuder-based system, Huanjing Kexue 8 (38) (2017) 3605–3609, https://doi.org/10.13227/j.hjkx.201701177. Chinese (9).

[51] W.J. Guan, X.Y. Zheng, N.-S. Zhong, Industrial pollutant emission and the major smog in China: from debates to action, The Lancet Planetary Health 1 (2) (2017) e57, https://doi.org/10.1016/S2542-5196(17)30024-4.

[52] S. Gligorovski, R. Strekowski, S. Barbati, D. Vione, Environmental implications of hydroxyl radical (•OH), Chem. Rev. 115 (24) (2015) 13051–13092, https://doi.org/10.1021/cr500310b.

[53] V.V. Mehmeti, A.R. Berisha, Corrosion study of mild steel in aqueous sulfuric acid solution using 4-methyl-4H-1,2,4-Triazole-3-Thiol and 2-mercaptonicotinic acid—an experimental and theoretical study, Front Chem 5 (2017) 61, https://doi.org/10.3389/fchem.2017.00061.

[54] A.K. Singh, S.K. Shukla, M.A. Quraishi, Corrosion behavior of mild steel in sulphuric acid solution in presence of ceftazidime, Int. J. Electrochem. Sci. 6 (2011) 5802–5814.

[55] E.A. Noor, A.H. Al-Moubaraki, Corrosion behavior of mild steel in hydrochloric acid solutions, Int. J. Electrochem. Sci. 3 (2008) 806–818.

[56] R. Hasanov, M. Sadikoğlu, S. Bilgiç, Electrochemical and quantum chemical studies of some Schiff bases on the corrosion of steel in H_2SO_4 solution, Appl. Surf. Sci. 253 (8) (2007) 3913–3921.

[57] P.B. Mathur, T. Vasudevan, Reaction rate studies for the corrosion of metals in acids-I, iron in mineral acids, Corrosion 38 (3) (1982) 171–178.

[58] Q. Kun, Y. Chiaki, Nitration of aromatic compounds with Nitric acid catalyzed by ionic liquids, Chemistry letter 33 (7) (2004) 808–809, https://doi.org/10.1246/cl.2004.808.

[59] M. Deborde, U. von Gunten, Reactions of chlorine with inorganic and organic compounds during water treatment —kinetics and mechanisms: a critical review, Water Res. 42 (1–2) (2008) 13–51.

[60] J.D. Burley, H.S. Johnston, Ionic mechanism for heterogeneous stratospheric reactions and ultraviolet photoabsorption cross sections for NO_2^+, HNO_3 and NO_3^- in sulfuric acid, Geophys. Res. Lett. 19 (13) (1992) 1359–1362, https://doi.org/10.1029/92GL01115. Correction, 19, 14 (2012) 1527-1527.